Implementation of Neoclassical Effects in Momentum Transport Analysis at LHD

Jasper BECKERS, Katsumi IDA[1,2], Mikirou YOSHINUMA[1], Masahiko EMOTO[1], Ryosuke SEKI[1], Masayuki YOKOYAMA[1,2] and Roger JASPERS

Eindhoven University of Technology, P.O. Box 513, 5600 MB Eindhoven, The Netherlands
[1]*National Institute for Fusion Science, 322-6 Oroshi Toki 509-5292, Japan*
[2]*SOKENDAI, 322-6 Oroshi, Toki 509-5292, Japan*

(Received 5 November 2016 / Accepted 21 January 2017)

Plasma rotation plays an important role in the suppression of turbulence, leading to an increase in energy and particle confinement. Significant rotation also leads to a stabilisation of the resistive wall mode. The external momentum input from Neutral Beam Injection (NBI) in current generation fusion plasmas may not be available for future self-heated fusion reactors. Therefore it is important to analyse the phenomenon of spontaneous rotation. At NIFS plasma rotation and momentum transport of the Large Helical Device (LHD) plasma is analysed using a code suite called TASK3D-a. In this work neoclassical effects, which can be especially significant in non-axisymmetric plasmas, were implemented in TASK3D-a. Initial analysis of neoclassical radial momentum flux profiles shows that in NBI-driven momentum input neoclassical effects, especially neoclassical damping, become dominant in the non-center plasma region. It was also found that during and after pellet-injection the neoclassical damping force becomes strong. With the implementation of neoclassical effects new features can be examined in the momentum flux-gradient relations; in the damping-dominated situation following pellet injection a large excursion in momentum flux is found. This work can aid in the search for neoclassical transport-optimised configurations for enhanced (spontaneous) plasma rotation.

Keywords: momentum transport, neoclassical viscosity, neoclassical driving torque, bulk-ion/impurity velocity difference, momentum flux-gradient relation

DOI: 10.1585/pfr.12.1402006

1. Introduction

Strong rotational flow shear can give rise to a suppression of turbulence (turbulent eddies are torn apart) leading to a reduction in transport and an increase in energy and particle confinement [1, 2]. Additionally, significant rotational velocity plays a role in the stabilisation of the resistive wall MHD mode. In an ideal (perfectly conducting) wall scenario the kink mode will be stabilised resulting in an increase in the maximum sustainable β. However, in practice the wall will always have a finite conductivity and as such eddy currents will cause the resistive wall mode. It has been shown that rotational velocity above a certain threshold can stabilise this mode and allow for a larger β to be achieved [3]. In current generation fusion plasmas rotation is usually provided by external momentum input from Neutral Beam Injection (NBI). However, this may not be available for future self-heated fusion reactors. Thus optimisation of the phenomenon of intrinsic torque [4] is important. For the Large Helical Device (LHD) the transport analysis suite TASK3D-a has been developed [5]. A limitation of the momentum transport code has been the absence of neoclassical effects, which can be especially significant in the non-axisymmetric plasma of LHD. In this paper the implementation of neoclassical effects in TASK3D-a is presented, along with initial observations of the momentum flux profiles and momentum flux-gradient relations. The evolution of these momentum fluxes is caused by exchange of NBI direction, for instance from co- to counter-direction or from balanced to counter, or by pellet injection. Additionally, the code was adapted for the momentum transport analysis of hydrogen as opposed to impurity species.

This paper is organised as follows. Chapter 2 presents an overview of momentum transport, the observation of spontaneous rotation and momentum transport analysis at LHD. Chapter 3 discusses the neoclassical effects that play a role in momentum transport, and the difference in rotation between bulk ions and impurities. In chapter 4 the implementation of neoclassical effects in the momentum transport analysis is described. Finally, initial results of the inclusion of neoclassical effects are presented in chapter 5.

2. Plasma Rotation

2.1 Momentum transport

Momentum transport is complex, especially in non-axisymmetric plasmas such as in LHD. A schematic overview of radial toroidal momentum transport can be

author's e-mail: j.p.beckers@student.tue.nl

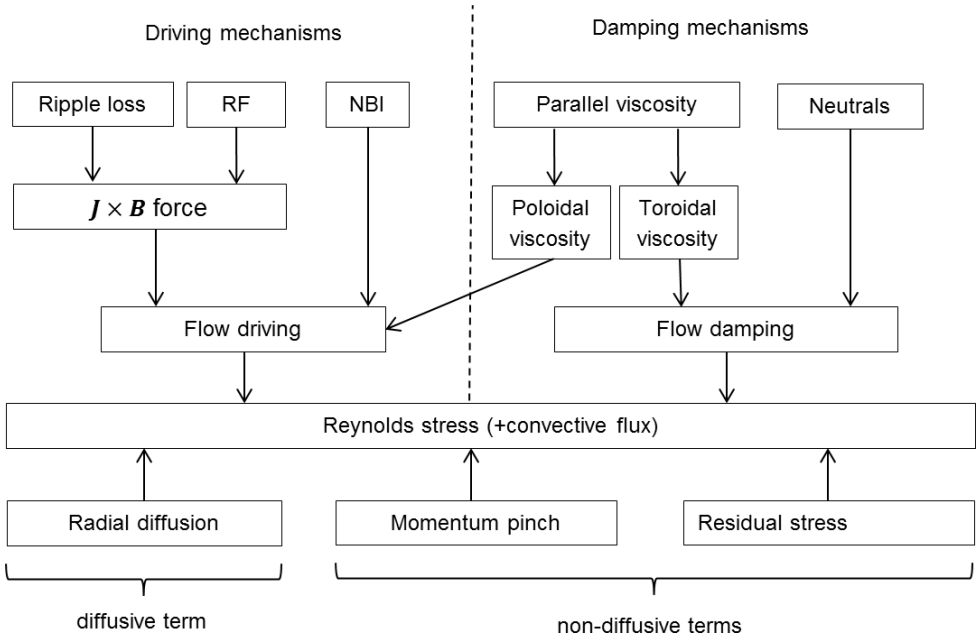

Fig. 1 Schematic overview of radial momentum transport. The upper left and right portions contain the main driving and damping mechanisms, respectively. These mechanisms lead to either flow driving or flow damping torques, which are balanced by the Reynolds stress and convective flux. The bottom shows the breakdown of the Reynolds stress in schematic form. Source: [6], modified.

seen in Fig. 1. Several driving and damping mechanisms interact with the plasma. It is important to distinguish the difference between a driving term in the counter-direction and a damping term. Driving terms can lead to an increase or decrease of rotational velocity depending on the driving direction (co- or counter-flow). They can either be collisional, such as NBI, or interact with the plasma through $\vec{J}\times\vec{B}$ torque. Torque directly connected to the flow velocity is considered a damping term. Collisional damping occurs due to the interaction with neutrals. Viscous forces in the plasma lead to a direct damping of toroidal velocity and also a damping of poloidal velocity. Due to the coupling between toroidal and poloidal rotation this can indirectly drive toroidal flow.

The driving and damping forces are balanced by the Reynolds stress and convective diffusion, the underlying physical mechanisms of momentum transport. The radial toroidal momentum balance equation for bulk ions is [6]

$$\nabla P_\phi(r) = T_\phi(r) - \frac{d[m_i n_i v_\phi^H(r)]}{dt}, \tag{1}$$

where P_ϕ is the momentum flux, T_ϕ is the toroidal torque input and the last term is the momentum temporal derivative with m_i, n_i and v_ϕ^H being the ion mass, ion density and toroidal hydrogen velocity, respectively. The total torque T_ϕ is the sum of the driving and damping torques.

The momentum flux P_ϕ consists of a convective term and the toroidal Reynolds stress term:

$$P_\phi = \underbrace{m_i v_\phi^H(r)\langle v_r^H n_i\rangle}_{\text{convective flux}} + \underbrace{m_i n_i \langle v_r^H v_\phi^H\rangle}_{\text{Reynolds flux}}, \tag{2}$$

where v_r^H is the radial hydrogen velocity.

The convective momentum flux can be neglected in regions with strong fuelling, among them the ionisation region near the edge. The second term, the Reynolds momentum flux, is dominant and can be separated into diffusive and non-diffusive terms. It is important to note that the Reynolds stress cannot lead to a net momentum change but merely a redistribution.

$$\langle v_r^H v_\phi^H\rangle = \underbrace{-\mu_\perp \nabla v_\phi^H}_{\text{diffusive term}} + \underbrace{v_{pinch} v_\phi^H + \Gamma_\phi}_{\text{non-diffusive terms}}. \tag{3}$$

The diffusive term arises from a gradient in toroidal velocity. The perpendicular viscosity $\mu_\perp$ causes a toroidal momentum flux in regions of radial velocity shear. The non-diffusive terms are the momentum pinch term (with v_{pinch} being the pinch velocity), scaling with the toroidal bulk ion velocity, and the residual stress term denoted by Γ_ϕ. Momentum pinch causes peaking of the toroidal velocity profile regardless of rotation direction via an inward momentum flow and is the subject of active research. Two major models are based on turbulent equipartition (TEP model) [7] and on the Coriolis force, respectively. The TEP model explains the inward momentum pinch by the fact that in a uniform radial momentum distribution velocity will increase towards flux surfaces with lower root mean square radii (ie. towards the center).

Residual stress is regarded as an off-diagonal element in the transport matrix. Residual stress produces momentum flux driven by temperature or pressure gradients and is not yet fully understood. Examining off-diagonal ele-

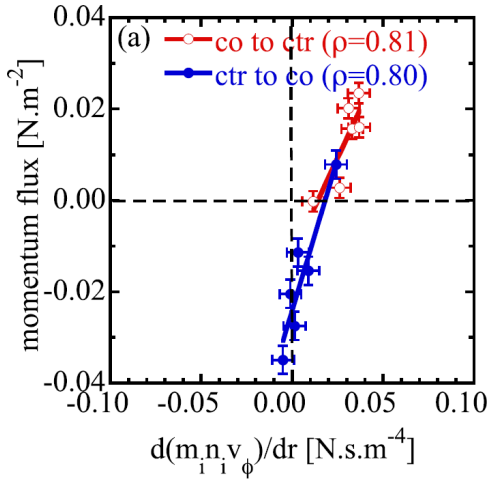

Fig. 2 Momentum flux-gradient plot, axis offset can indicate spontaneous rotation. Source: [8].

ments in momentum transport can be done by means of a flux-gradient plot as shown in Fig. 2. The co- and counter-directions are defined with respect to the plasma current direction, or alternatively the poloidal magnetic field direction. Measurements are taken near the edge during a reversal in rotation, induced by an exchange of NBI direction or a pellet injection. The convective momentum flux and momentum pinch terms can be neglected due to edge ionisation and low toroidal velocity, respectively. This allows for examination of the toroidal diffusive viscosity and the non-diffusive viscosity due to the residual stress. The diffusive viscosity is proportional to the slope of the curve in the flux-gradient plot while the non-diffusive term is proportional to the offset. This offset is due to the residual stress being an off-diagonal element in the momentum transport matrix.

2.2 Spontaneous rotation

In a momentum flux-gradient plot (Fig. 2) it can be seen that a finite momentum flux exists even at zero velocity gradient, and similarly a velocity gradient exists at zero momentum flux. This indicates an intrinsic and spontaneous toroidal rotation. The existence of intrinsic rotation has been confirmed in experiments with ohmic discharges [9], where there is no external momentum input, as well as in experiments with balanced external momentum input [10]. Especially in self-heated plasmas, without external momentum input through NBI or pellet injection, spontaneous torque can aid in producing plasma rotation.

2.3 TASK3D-a analysis suite at LHD

TASK3D-a is the integrated transport analysis suite for toroidal helical plasmas used at LHD [5]. It is based on TASK for two-dimensional configurations [11]. The TASK3D-a suite consists of several code modules for different areas of analysis. The energy and momentum balance module is called DYTRANS (dynamic transport) [12]. A limitation of DYTRANS has been the fact that it does not take into account neoclassical viscosity (damping torque) and the neoclassical driving force. Here an implementation of these effects is presented along with an initial analysis of the results. The implementation is analytical, based on plasma parameters. DYTRANS was also adapted to make the analysis of hydrogen momentum transport possible, as opposed to impurity momentum transport.

3. Neoclassical Momentum Transport Theory

3.1 Neoclassical toroidal viscosity and driving force

In axisymmetrical plasmas the parallel neoclassical viscosity is small, but for non-axisymmetric plasmas it can be significant. In neoclassical theory the viscosity, μ_ϕ^{NC}, is dependent on the thermal velocity v_{th} and a geometric factor of the magnetic field λ [13]:

$$\mu_\phi^{NC} = 2\frac{v_{th}J}{\lambda R B_\phi}, \tag{4}$$

where J, R and B_ϕ are the poloidal current, major radius and toroidal magnetic field strength, respectively.

Neoclassical toroidal viscosity decreases toroidal rotation and disperses momentum. The damping force density d_ϕ^{NC} is given by

$$d_\phi^{NC} = n_e m_i v_\phi^H \mu_\phi^{NC}, \tag{5}$$

where v_ϕ^H is the rotational hydrogen velocity.

The neoclassical driving force is defined as the force required to balance the neoclassical viscous force at the neoclassical toroidal velocity v_ϕ^{NC}, which is calculated with the explicit expressions for non-axisymmetric plasmas [14, 15]. Both the neoclassical poloidal and toroidal rotation are a function of the neoclassical radial electric field. The neoclassical driving force is defined by

$$f_\phi^{NC} = n_e m_i v_\phi^{NC} \mu_\phi^{NC}, \tag{6}$$

where f_ϕ^{NC} is the neoclassical force density and μ_ϕ^{NC} the neoclassical viscosity. In tokamak terminology this driving force is called NTV (Neoclassical Toroidal Viscosity) torque. Neoclassical ripple loss due to strong magnetic field wells in non-axisymmetric plasmas leads to an enhanced radial current. This neoclassical radial current can drive rotation in the plasma via $\vec{J}\times\vec{B}$ torque.

3.2 Rotations of bulk ions and impurities

It has been found that the rotation of impurities is different than that of hydrogen [16]. This leads to a velocity correction, $\Delta v_\phi^{H,C} = v_\phi^H - v_\phi^C$, required for the analysis of bulk ion (hydrogen) transport. This is necessary since the diagnostic of charge exchange spectroscopy measures

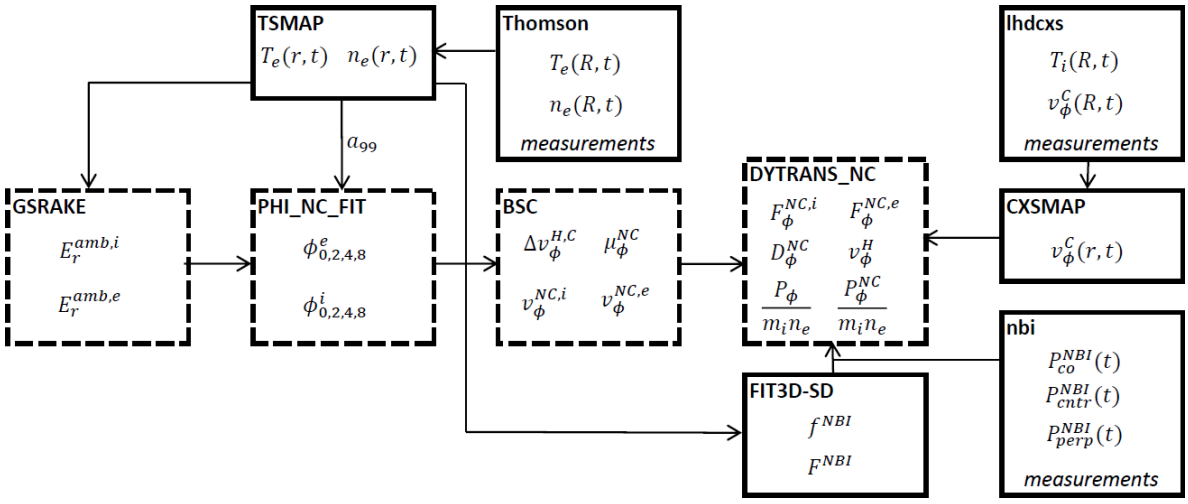

Fig. 3 Schematic overview of the implementation of neoclassical effects in the TASK3D-a module suite. Dash-outlined modules are new modules, whereas original modules are outlined by solid lines. As TASK3D-a is an extensive suite not all external inputs are shown.

only impurity rotation. Two effects contribute to the difference in rotation: one is the difference in diamagnetic flow and the other is the thermodynamic force due to the ion temperature gradient. The correction factor is a function of the normalised geometric factor $\langle G \rangle$. $\langle G \rangle$ depends on the collisionality regime, radius and magnetic axis position. For axisymmetric plasmas it is always unity, but not for non-axisymmetric plasmas. In the $1/\nu$ regime the factor depends strongly on the field structure, where ν is the collisionality. In the plateau regime the factor is generally small and in the Pfirsch-Schlüter regime it is very small.

4. Implementation in TASK3D-a

In order to incorporate the neoclassical viscous damping and driving forces, Eqs. (5) and (6), respectively, into the dynamic transport analysis code DYTRANS a few new modules were added to the suite. An overview of these additions can be seen in Fig. 3.

4.1 GSRAKE

Firstly the GSRAKE module was added for registration to the data server of the neoclassical radial electric field (see Table 1 for output variables). The neoclassical electric field is obtained with the General Solution of the Ripple-Averaged Kinetic Equation (GSRAKE) code [17]. The input for this code is electron temperature and density data from the TSMAP module, which converts measurement values from the Thomson module from real coordinates to flux coordinates. The GSRAKE code output may have multiple solutions of the electric field, some of which can be unstable. An effort to automatically select the stable continuous electron (positive, denoted by $E_r^{amb,e}$) and ion (negative, $E_r^{amb,i}$) root was made. Therefore the module registers both the electron and ion roots of the neoclassical electric field and is zero if no corresponding root is found in the original output. There exists a transition from the small negative electron root to the positive ion root when the density (and consequently plasma collisionality) decreases beyond a certain critical value [18]. However, this was not implemented into the module and the physical root is ought to be selected manually.

4.2 PHI_NC_FIT

Registered GSRAKE output is read by the module PHI_NC_FIT, which calculates the neoclassical radial potential profiles for both the electron and ion root (denoted by ϕ^e and ϕ^i). Hereby, in order to obtain the normalised minor radius, the value a_{99} is read from the module TSMAP. This value is defined as the radius of the volume containing 99% of plasma energy. The coefficients of an 8^{th} order even polynomial fit of the potential profiles are registered to the data server.

4.3 BSC

The resulting neoclassical potential profiles from the PHI_NC_FIT module are read by the module BSC [15], which calculates the neoclassical viscosity and velocity according to the theory in 3.1. Whereas the neoclassical viscosity is purely a function of magnetic field modulation (and thus not a function of the radial electric field), the neoclassical velocity is dependent on the neoclassical electric field and thus has different results based on whether the electron or ion root solution is used. The output of the BSC data registration procedure consists of the neoclassical viscosity $\mu^{NC}_{\phi(\sim/\!/)}$ and the two solutions for the neoclassical toroidal velocity v_ϕ^{NC} for the ion and electron electric field roots. The hydrogen-impurity rotational velocity difference $\Delta v_\phi^{H,C}$ is also calculated.

Table 1 Output values of new modules. Some additional derived values are not shown.

a) GSRAKE

Variable	t	r_{eff}/a_{99}	$E_r^{amb,i}$	$E_r^{amb,e}$
Unit	s	-	kV/m	kV/m

b) PHI_NC_FIT

Variable	t	$\phi_{0,2,4,6,8}^{amb,i}$	$\phi_{0,2,4,6,8}^{amb,e}$
Unit	s	kV	kV

c) BSC

Variable	t	r_{eff}/a_{99}	$\Delta v_\phi^{H,C}$	$v_\phi^{NC,i}$	$v_\phi^{NC,e}$	μ_ϕ^{NC}
Unit	s	-	kms^{-1}	kms^{-1}	kms^{-1}	s^{-1}

d) DYTRANS_NC

Variable	t	r_{eff}/a_{99}	D_ϕ^{NC}	$F_\phi^{NC,i}$	$F_\phi^{NC,e}$	$\frac{P_\phi}{m_i n_e}$	$\frac{P_\phi^{NC}}{m_i n_e}$	v_ϕ^H
Unit	s	-	N	N	N	$10^3\ \mathrm{m^2 s^{-2}}$	$10^3\ \mathrm{m^2 s^{-2}}$	kms^{-1}

4.4 DYTRANS_NC

DYTRANS_NC is the name of the dynamic transport module after the modification for neoclassical effects. It reads the registered output of the BSC module. Additionally impurity rotational velocity is obtained from the CXSMAP module, which converts the charge exchange spectroscopy data to flux coordinates. The bulk ion velocity v_ϕ^H is then calculated by incorporating $\Delta v_\phi^{H,C}$. The neoclassical damping and driving force densities are evaluated according to Eqs. (5) and (6), respectively. It follows that the damping force is obtained using experimental velocity profiles and numerical computations based on plasma parameters. The driving force is obtained purely by computation of the neoclassical viscosity and velocity. Volume integration of these force densities gives the neoclassical damping and driving forces, D_ϕ^{NC} and F_ϕ^{NC}. Momentum flux follows from the volume integrated force over the volume derivative $\frac{\partial V}{\partial r_{eff}}$. NBI power and momentum input forces are read from the nbi and FIT3D-SD [19] modules, respectively. By evaluation of Eq. (1), force density surface integration, the normalised radial flux of toroidal momentum $P_\phi^{NC}/m_i n_e$ is obtained, with neoclassical effects taken into account. The non-neoclassical momentum flux is also registered to the data server.

5. Results

Here initial results of the implementation of neoclassical effects in momentum transport analysis code DYTRANS_NC are presented. First it is shown that the neoclassical viscosity profile behaves as expected and agrees with previous computational results. Next it is shown that the found neoclassical momentum fluxes are in agreement with experimental observations. Finally new features in the neoclassical flux-gradient relations are presented.

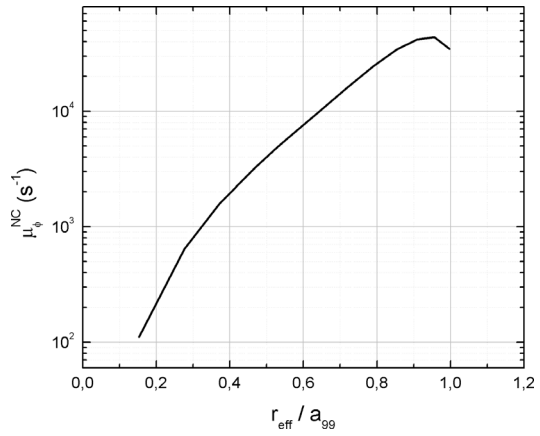

Fig. 4 Computed neoclassical toroidal viscosity in LHD discharge 105992. The viscosity rises more than two orders of magnitude from the plasma center to the edge.

5.1 Neoclassical viscosity in LHD discharges

The neoclassical viscosity profile depends for the most part on the magnetic field configuration and as such there are only relatively small differences between the shots. Computation of the radial neoclassical viscosity profile for LHD discharge 105992 shows an increase in viscosity towards the edge of the plasma of more than two orders of magnitude, see Fig. 4. This increase is expected as the magnetic field modulation increases towards the edge, especially in non-axisymmetric plasmas such as

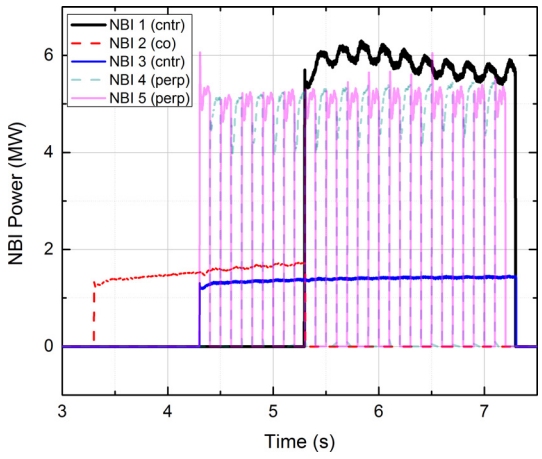

Fig. 5 NBI power profile. Beam #1 through #3 are tangentially injected. The co- and counter-directions are defined in relation to the toroidal magnetic field axis. In discharge 111099 the magnetic field is $B_\phi = +2.68$ T. Beam #4 and #5 are perpendicularly injected and for diagnostic purposes. Here the NBI in the co-direction is injected from t = 3.3 - 5.3 s, and the NBIs in the counter-direction are injected from t = 4.3 - 7.3 s and 5.3 - 7.3 s.

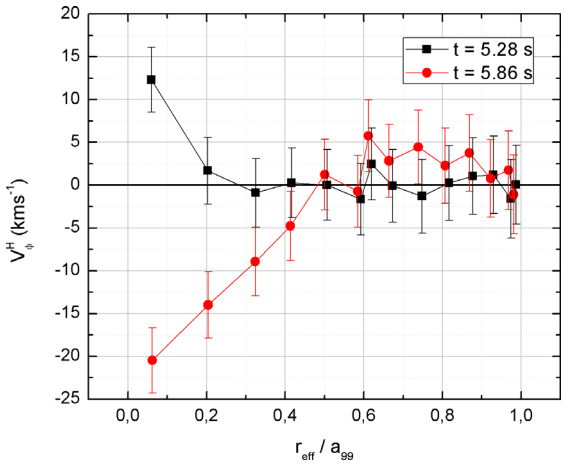

Fig. 6 Rotational bulk ion CXS velocity profile comparison before and after the start of counter-directional momentum input ($t = 5.275$ s and $t = 5.855$ s of discharge 111099, respectively). Velocity is corrected for the hydrogen-impurity rotation difference, see Sec. 3.2.

in LHD. The neoclassical viscosity at the core region is low because at that position the magnetic field can be regarded near axisymmetric and consequently field modulation, which leads to neoclassical viscosity, is small. The result is in agreement with the neoclassical toroidal viscosity profile of the Compact Helical System (CHS) torsatron/heliotron device for the plateau regime [13, Fig. 2], a device with similar magnetic field configuration and geometry.

5.2 Neoclassical force profiles

Momentum transport is analysed in non-steady state situations, where changes in velocity occur. The magnitude of neoclassical effects was examined for two discharges with different causes of velocity change. In the first discharge (111099) this is a change in NBI power as can be seen in Fig. 5. In the initial state there is a balance of momentum input. Beams with opposite injection direction, #2 (co-direction) and #3 (counter-direction), are injected at similar power levels resulting in near-zero momentum input. At $t = 5.3$ s NBI beam #2 is disengaged and #1 is injected at a power of almost 6 MW, creating a counter-directional torque. This leads to an increase in toroidal hydrogen velocity in the counter-direction as can be seen in Fig. 6.

In both situations the velocity profile is peaked towards the center of the plasma. The flow at radii larger than the normalised plasma radius $r_{eff}/a_{99} \approx 0.5$ is small regardless of the activation of the NBI momentum input. Here r_{eff} is the effective radial position and a_{99} is defined as the radius of the volume containing 99% of the plasma energy. This is in agreement with the large toroidal viscosity in the outer plasma regions (see 5.1).

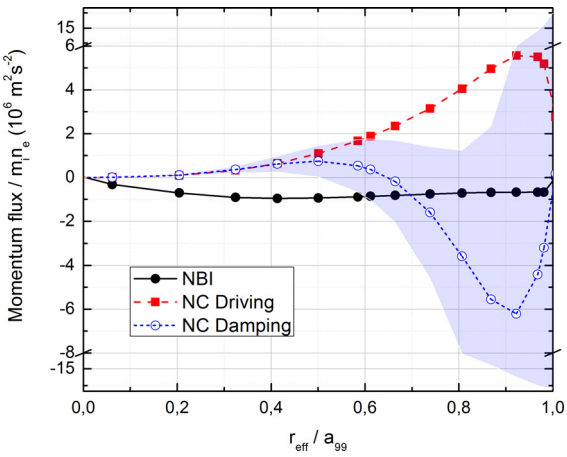

Fig. 7 Profile of radial momentum fluxes due to NBI injection and neoclassical damping and driving (ion root) forces after the injection of NBI beam #1 in the counter-direction (at $t = 5.855$ s, shot 111099). The error interval for neoclassical damping flux is shaded.

A comparison between the neoclassical and NBI-induced momentum fluxes can be seen in Fig. 7. The counter-directional NBI force density, gradient of the NBI momentum flux, is strongest in the plasma center and decreases outwards. The neoclassical damping momentum flux is small in the plasma center because the neoclassical viscosity is not large at that position. The viscosity increases towards the edge and so does the damping flux. The damping momentum flux is positive, dampening the NBI-induced counter-rotation, and starts to drop after the radius $r_{eff}/a_{99} \approx 0.5$, where the rotational bulk ion velocity flips sign (see Fig. 6). Due to the integration of the error in the velocity measurement the neoclassical

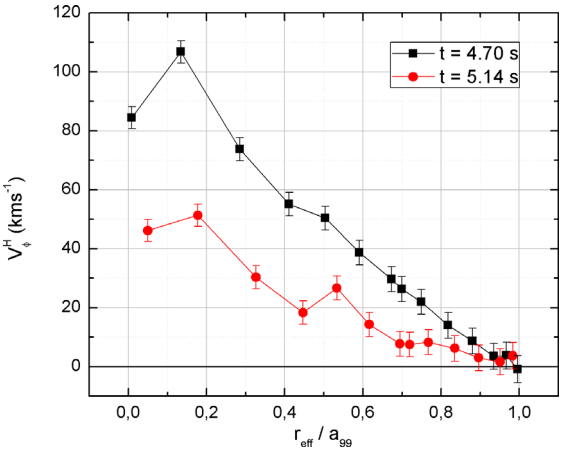

Fig. 8 Radial profile of CXS toroidal hydrogen velocity of discharge 113288 shortly after pellet injection and 0.44 s later (at t = 4.70 s and at t = 5.14 s, respectively). Velocity corrected for the hydrogen-impurity difference (Sec. 3.2). The injected NBI beam power is co-dominant from t = 4.5 - 4.7 s and 4.8 - 5 s and balanced from t = 4.7 - 4.8 s.

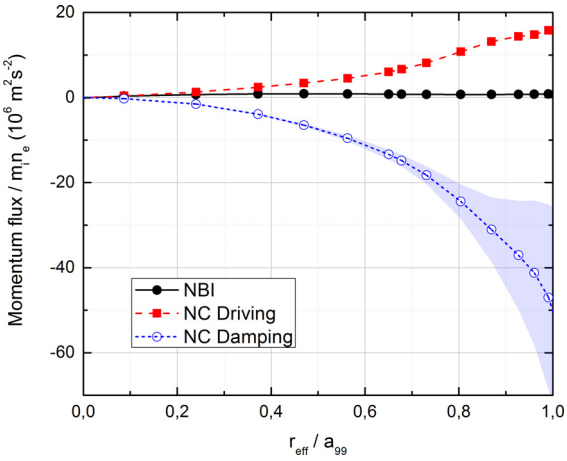

Fig. 9 Profile of radial momentum fluxes due to NBI injected force and neoclassical damping and driving (ion root) forces of shot 113288 at t = 4.818 s. Due to the large rotation shortly after pellet injection neoclassical damping is dominant along the entire profile. The NBI injected power is co-dominant. The error interval for neoclassical damping flux is shaded.

damping flux error becomes increasingly large towards the edge. The damping momentum flux increases negatively due to the magnitude of the neoclassical viscosity. In the outer regions the neoclassical damping momentum flux becomes more dominant than the NBI-induced momentum flux, which diminishes in the outer half of the plasma. From the GSRAKE code follows a continuous negative ion root for the neoclassical ambipolar radial electric field, whereas the electron root solution is mostly non-existent. Therefore the ion root solution of the neoclassical driving flux is shown as opposed to the electron root. The positive momentum flux from co-directional driving force increases towards the outer plasma, providing a momentum flux balance against the fluxes from NBI and damping.

In the balanced state prior to counter-directional flow no net NBI momentum input exists and neoclassical damping momentum flow is smaller than 10^6 [m^{2}s^{-2}]. The driving momentum flow in the outer plasma region is of equal magnitude as in the state after counter-directional NBI injection. This is because the neoclassical velocity in the center is large in both cases, > 80 [kms^{-1}].

Besides NBI beams another method that can be used to impart plasma momentum is pellet injection. This is suitable in momentum transport analysis as it provides a large change in rotational velocity in the entire plasma and on timescales smaller than that of momentum dispersion (see Fig. 8). This is in contrast to NBI-induced velocity change, which occurs primarily in the plasma center and is not as instantaneous. In discharge 113288 a pellet is injected in the co-direction in a co-NBI heated plasma, creating a positive toroidal rotation. In the initial co-dominant state there exists neoclassical damping and driving flux at the edge of equal size but opposite sign, forming a balance. Figure 8 shows the increase in toroidal velocity. At the velocity peak, t = 4.70 s, shortly after pellet injection the toroidal hydrogen rotation reaches $v_\phi^H = 107$ [kms^{-1}]. Figure 8 also shows that the toroidal velocity drops after the initial rise. This is due to the strong damping. The momentum flux due to neoclassical damping force is dominant along the entire plasma radius as can be seen in Fig. 9 and increases towards the edge where neoclassical viscosity has a value of 3.6×10^4 [s^{-1}]. The neoclassical driving momentum flux established with the ion root of the neoclassical ambipolar radial electric field is also shown. Similar to the damping-induced momentum flux there is a gradual increase towards the outer regions but not of sufficient magnitude to provide a flux balance. The neoclassical damping force is strongly dominant in this case, when compared to the NBI injection case.

5.3 Flux-gradient relation including neoclassical effects

With the implementation of the neoclassical damping and driving terms in `TASK3D-a` the effect on the momentum flux-gradient plot can be examined. For a discharge such as 111099, with a change in NBI momentum input, a transition between two states is clearly visible. The time evolution of the bulk ion velocity at a radius of $r_{eff}/a_{99} \approx 0.2$ can be seen in Fig. 10. The rotation is low until the strong counter-directional torque from NBI #1. The toroidal velocity drops and becomes negative until it settles at roughly $v_\phi^H \approx -17$ [kms^{-1}]. These two states can also be identified in the bulk ion momentum flux-gradient relation as seen in Fig. 11. The relations with only NBI momentum input (labelled *NBI*) and with both NBI and neoclassical momentum input taken into account (labelled

Total) are shown. Because flow velocity is damped in the outer plasma regions (see Fig. 6) the flux-gradient relation can best be visualised in the area of larger velocity difference, in this case closer to the center. The flux-gradient relation is therefore visualised at a radius of $r_{eff}/a_{99} \approx 0.2$. As expected, and not influenced by neoclassical effects, the velocity gradient in the initial state is negative and becomes positive after the rotational change. During the change of flow in the counter-direction the velocity gradient increases significantly until peaking at $t \approx 5.5$ s. Finally it settles at a value of $\frac{dv_\phi^H}{dr_{eff}} \approx 2.5 \times 10^4$ [s^{-1}].

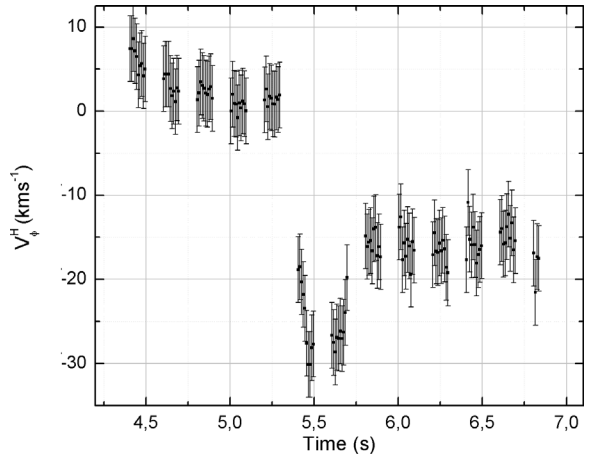

Fig. 10 Time evolution of toroidal hydrogen velocity at a radius of $r_{eff}/a_{99} \approx 0.2$, shot 111099. From $t = 5.3$ s on a strong counter-directional force is imparted on the plasma (see Fig. 5) leading to a negative toroidal velocity.

It can be seen that the momentum flux in the initial state is larger when neoclassical effects are taken into account. Initially there is a small positive rotation (see Fig. 10) causing a small neoclassical damping force in the counter-direction. The neoclassical driving force is in the co-direction and of larger magnitude, causing positive momentum flow in the initial state. This effect is not present in the NBI-only case. Next the change of NBI power lowers the momentum flux, in both cases. During the growth of counter-directional bulk ion velocity the neoclassical damping force increases in the co-direction and consequently the difference in momentum flux between the NBI-only flux-gradient relation and the one with neoclassical effects taken into account increases. In the final steady, slightly weaker toroidal velocity state damping decreases. At the end of the discharge a rise in neoclassical viscosity occurs causing an increased co-directional damping force. This is reflected in the increase in momentum flux at the end of the flux-gradient relation.

The time evolution of toroidal hydrogen velocity of discharge 113288 can be seen in Fig. 12, after pellet injection at $t = 4.6$ s. Figure 13 shows the radial flux-gradient relation of toroidal bulk ion momentum. Even at a radius of roughly $\rho \approx 0.5$ a clear change in momentum gradient can be seen. This is indicative of the strong pellet-induced torque which is sufficient to overcome the relatively large plasma viscosity in this outer plasma region. Initially the hydrogen velocity gradient is small and rises to an extreme

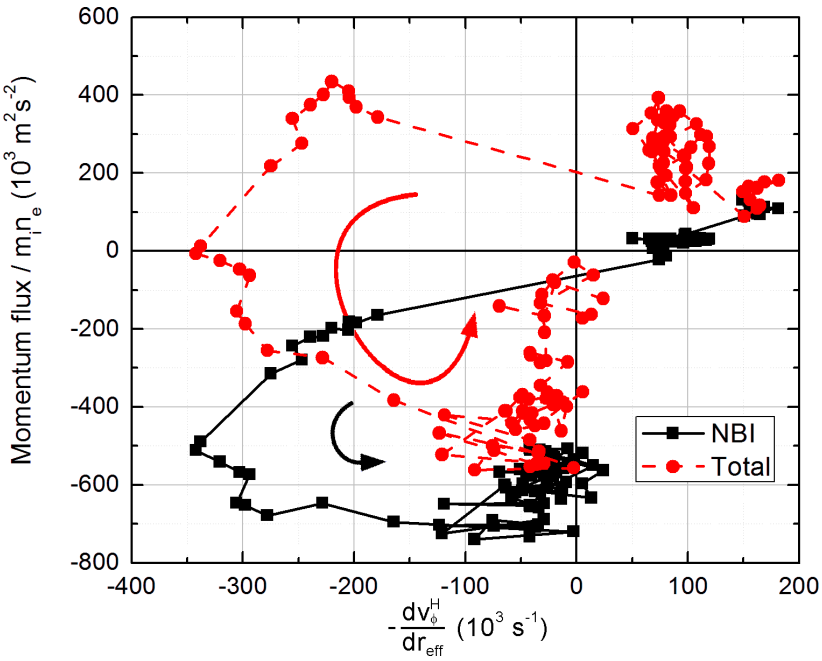

Fig. 11 Radial flux-gradient plot of toroidal hydrogen momentum at a radial position of roughly $\rho \approx 0.2$, showing the profile during the NBI power change in shot 111099. Both the non-neoclassical, with only NBI momentum input taken into account, and neoclassical trajectories are shown. As is convention the horizontal axis shows negative bulk ion velocity gradient.

of nearly $\frac{dv_\phi^H}{dr_{eff}} \approx -3.5 \times 10^5$ [s^{-1}] after pellet injection. As can be seen in Fig. 12 the measured toroidal bulk ion velocity after pellet injection has a large scatter, which is reflected in the scatter of the momentum gradient after pellet injection.

Due to the original momentum flux just taking into account NBI momentum input the consequence of large neoclassical damping force is not reflected in the original flux-gradient relation. The new profile shows a strong negative momentum flux due to dominant neoclassical damping in the counter-direction, up to $\approx -1 \times 10^7$ [$m^2 s^{-2}$], at the end of the velocity rise (at $t \approx 4.71$ s). This momentum flux excursion after the pellet injection is not discernible when neoclassical effects are not taken into account. After the peaking of velocity the momentum flux, taking neoclassical effects into account, starts decreasing in magnitude and ultimately becomes very small. This is in contrast to the pure-NBI momentum flux, which shows a relatively large positive momentum flux during and after the pellet injection. A small value of momentum flux is expected in the final steady state.

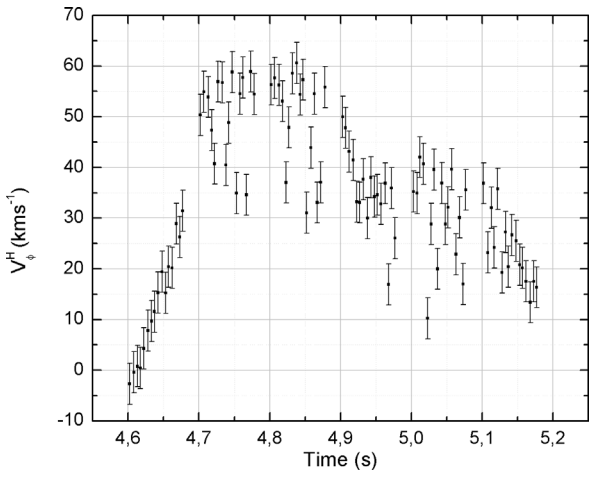

Fig. 12 Time evolution of toroidal hydrogen velocity at $r_{eff}/a_{99} \approx 0.5$, shot 113288. The velocity rises quickly after pellet injection at $t = 4.6$ s and drops after peaking around $t = 4.75$ s.

6. Conclusion and Future Work

Neoclassical effects, specifically neoclassical toroidal damping and driving terms, were implemented in the TASK3D-a analysis suite at LHD. This required the creation of additional modules to handle the calculation and data registration of new variables. The implementation is analytical, based on plasma parameters. The calculation of neoclassical toroidal viscosity profiles shows an increase of multiple orders of magnitude towards the plasma edge. This is due to the increasingly large magnetic field modulation caused by the non-axisymmetry of LHD. The consequence of this is generally an increase of magnitude of neoclassical effects towards the edge. Radial neoclassical force and momentum flux comparisons can now be made and initial analysis shows that in NBI-driven discharges neoclassical momentum flux can, especially neoclassical damping, become dominant in the non-center plasma region (for the examined discharge from a radius of

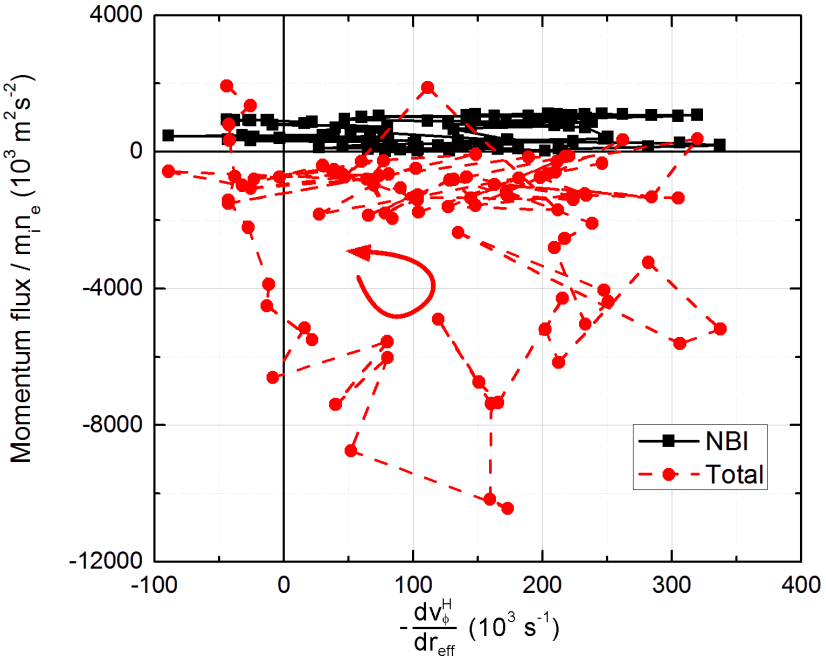

Fig. 13 Radial flux-gradient plot of toroidal hydrogen momentum at a radial position of roughly $\rho \approx 0.5$ during and after pellet injection, shot 113288. Both the non-neoclassical, with only NBI momentum input taken into account, and neoclassical phase trajectories are shown. The horizontal axis shows negative bulk ion velocity gradient.

$r_{eff}/a_{99} \approx 0.5$). Another indication of strong neoclassical effects is found in a shot during and after pellet-injection, where the neoclassical damping flux becomes very strong due to the large, plasma-wide change in velocity.

With the implementation of neoclassical effects new features can be examined in the momentum flux-gradient relations. For instance in the damping-dominated situation following pellet injection a large excursion in momentum flux is found.

Future work can focus on the configuration and plasma parameter dependence of neoclassical effects for the optimisation of (spontaneous) rotation in future and present devices. The newly implemented neoclassical effects can also act as a bridge between `FORTEC-3D` simulation code [20] results, which is limited to the situation without external momentum input, and experimental results.

Acknowledgements

The authors are grateful to the LHD Experiment Group for making the experimental data available, and to the TASK3D-UD (users and developers) colleagues for making this successive transport analysis possible. Finally one of the authors, J.B., would like to thank NIFS for hosting him and FuseNet (the European Fusion Education Network) for providing funding for his stay.

[1] R. Groebner *et al.*, Phys. Rev. Lett. **64**, 3015 (1990).
[2] K. Ida *et al.*, Phys. Rev. Lett. **65**, 1364 (1990).
[3] A. Garofalo *et al.*, Phys. Rev. Lett. **89**, 235001 (2002).
[4] K. Ida *et al.*, Phys. Rev. Lett. **74**, 1990 (1995).
[5] M. Yokoyama *et al.*, "Extended Capability of the Integrated Transport Analysis Suite, `TASK3D-a`, for LHD Experiment, and its Impacts on Facilitating Stellarator-Heliotron Research", 26th IAEA-FEC, Kyoto (Oct. 2016).
[6] K. Ida and J. Rice, Nucl. Fusion **54**, 045001 (2014).
[7] Ö. Gürcan *et al.*, Phys. Rev. Lett. **100**, 135001 (2008).
[8] K. Ida *et al.*, J. Phys. Soc. Jpn. **67**, 4089 (1998).
[9] J. Rice *et al.*, Nucl. Fusion **37**, 421 (1997).
[10] K. Ida *et al.*, Nucl. Fusion **50**, 064007 (2010).
[11] A. Fukuyama, TASK code, *http://bpsi.nucleng.kyoto-u.ac.jp/task/*
[12] H. Lee, K. Ida *et al.*, Plasma Phys. Control. Fusion **55**, 014011 (2013).
[13] K. Ida *et al.*, Phys. Plasmas **4**, 310 (1997).
[14] N. Nakajima and M. Okamoto, J. Phys. Soc. Jpn. **61**, 833 (1992).
[15] K. Watanabe *et al.*, Nucl. Fusion **35**, 335 (1995).
[16] N. Nakajima and M. Okamoto, J. Phys. Soc. Jpn. **60**, 4146 (1991).
[17] C.D. Beidler and W. D'haeseleer, Plasma Phys. Control. Fusion **37**, 463 (1995).
[18] K. Ida *et al.*, Phys. Rev. Lett. **86**, 5297 (2001).
[19] S. Murakami *et al.*, Fusion Technol. **27**, 256 (1995).
[20] S. Satake *et al.*, Nucl. Fusion **45**, 1362 (2005).